

Time-resolved Infrared Spectroscopy of the Ca^{2+} -ATPase

THE ENZYME AT WORK*

(Received for publication, June 25, 1996, and in revised form, August 30, 1996)

Andreas Barth[‡], Frithjof von Gerner[§], Werner Kreutz, and Werner Mäntele[§]

From the Institut für Biophysik und Strahlenbiologie der Universität Freiburg, Albertstrasse 23, D-79104 Freiburg, Germany

Changes in the vibrational spectrum of the sarcoplasmic reticulum Ca^{2+} -ATPase in the course of its catalytic cycle were followed in real time using rapid scan Fourier transform infrared spectroscopy. In the presence of Ca^{2+} , the cycle was induced by the photochemical release of ATP from a biologically inactive precursor (caged ATP, P^3 -1-(2-nitro)phenylethyladenosine 5'-triphosphate). Absorbance changes arising from ATP binding to the ATPase were observed within the first 65 ms after initiation of ATP release. After ATP binding, up to two subsequent partial reactions of the ATPase reaction cycle were observed depending on the buffer composition (10 mM CaCl_2 + 330 mM KCl or 1 mM CaCl_2 + 20% Me_2SO): (i) formation of the ADP-sensitive phosphoenzyme ($k_{\text{app}} = 0.79 \text{ s}^{-1} \pm 15\%$ at 1 °C, pH 7.0, 10 mM CaCl_2 , 330 mM KCl) and (ii) phosphoenzyme conversion to the ADP-insensitive phosphoenzyme concomitant with Ca^{2+} release ($k_{\text{app}} = 0.092 \text{ s}^{-1} \pm 7\%$ at 1 °C, pH 7.0, 1 mM CaCl_2 , 20% Me_2SO). Each reaction step could well be described by a single time constant for all associated changes in the vibrational spectrum, and no intermediates other than those mentioned above were found. In particular, there is no evidence for a delay between the transition from ADP-sensitive to ADP-insensitive phosphoenzyme and Ca^{2+} release. In $^2\text{H}_2\text{O}$ a kinetic isotope effect was observed: both the phosphorylation reaction and phosphoenzyme conversion were slowed down by factors of 1.5 and 3.0, respectively.

The small amplitudes of the observed changes in the infrared spectrum indicate that the net change of secondary structure is very small and of the same order of magnitude for ATP binding, phosphorylation, and phosphoenzyme conversion. Therefore, our results do not support a distinction between minor and major secondary structure changes in the catalytic cycle of the ATPase, which might be expected according to the classical E_1 - E_2 model.

The Ca^{2+} -ATPase of the SR¹ is an intrinsic membrane pro-

tein, which couples active Ca^{2+} -transport across the SR membrane to the hydrolysis of ATP. Its reaction cycle is shown in a simplified form in Fig. 1. Ca^{2+} is bound from the cytoplasmic side of the membrane to high affinity binding sites of the ATPase (step on the left of Fig. 1), which enables the ATPase to use ATP as a substrate (1). Phosphorylation by ATP (upper step in Fig. 1) results in the occlusion of the bound Ca^{2+} in the protein. The subsequent conversion of the phosphoenzyme from the ADP-sensitive to the ADP-insensitive form (step on the right of Fig. 1) leads to Ca^{2+} release into the SR lumen. Hydrolytic cleavage of the phosphoenzyme completes the reaction cycle (bottom step in Fig. 1). An ATP molecule is shown bound to the ATPase throughout the cycle, which is the case at millimolar ATP concentrations (reviewed in Ref. 2).

The original model of the reaction cycle from deMeis and Vianna (3) was based on the assumption of two main functional states, E_1 and E_2 , of the protein. The interconversion between E_1 and E_2 is thought to be associated with a reorientation of the Ca^{2+} -binding sites from the cytoplasmic side to the luminal side of the membrane and a change in reactivity of the phosphorylation site. However, Jencks and co-workers (4–7) questioned the existence of reaction intermediates of the E_1/E_2 model. They propose a switch mechanism in which Ca^{2+} binding and release switch the reaction specificity of the phosphorylation site, whereas phosphorylation and dephosphorylation switch the accessibility of the Ca^{2+} sites (5).

Infrared spectroscopy allows one to test the assumption that there are only two main conformations, E_1 and E_2 , in the ATPase reaction cycle which are interconverted by a major conformational change. Conformational changes of the protein will lead to changes in the amide I absorption of the polypeptide backbone, which is sensitive to secondary structure. This enables an estimate of the net change of secondary structure. According to the E_1 - E_2 model, we would expect relatively large changes of amide I absorption for the two steps involving Ca^{2+} binding or dissociation (vertical steps in Fig. 1) and only minor changes for the phosphorylation and dephosphorylation steps (horizontal steps in Fig. 1).

Detection of subtle changes in the vibrational spectrum between two enzyme states requires the sensitivity of FTIR spectroscopy and that the interconversion between the two states can be triggered in the infrared cuvette, for example by the photochemical release of effector molecules from inactive precursors (termed "caged compounds"). Using this approach, several steps of the Ca^{2+} -ATPase reaction cycle have been investigated (8–10) and infrared difference spectra were obtained, which show the difference between the initial state and the

ence spectrum calculated from a spectrum recorded at the indicated time interval after the photolysis flash and a reference spectrum recorded before the flash; E_1 and E_2 , functional states of the ATPase as described in the text; E_2 -P, ADP-insensitive phosphoenzyme; FTIR, Fourier transform infrared.

* The costs of publication of this article were defrayed in part by the payment of page charges. This article must therefore be hereby marked "advertisement" in accordance with 18 U.S.C. Section 1734 solely to indicate this fact.

[‡] Present address: National Institute for Medical Research, The Ridgeway, Mill Hill, London NW7 1AA, United Kingdom. Tel.: 44-181-959-3666; Fax: 44-181-906-4419.

[§] To whom correspondence should be addressed. Present address: Institut für Physikalische und Theoretische Chemie der Universität Erlangen-Nürnberg, Egerlandstrasse 3, D-91058 Erlangen, Germany.

¹ The abbreviations used are: SR, sarcoplasmic reticulum; AMP-PNP, β , γ -iminoadenosine 5'-triphosphate; caged AMP-PNP, P^3 -1-(2-nitro)phenylethyl β , γ -iminoadenosine 5'-triphosphate; caged ATP, P^3 -1-(2-nitro)phenylethyladenosine 5'-triphosphate; Ca_2E_1 -P, ADP-sensitive phosphoenzyme; COBSI, change of backbone structure and interaction (calculated as described in the text); ΔA (time interval), infrared differ-

final state or the steady state accumulating after release of the effector molecules. The time resolution previously available in such experiments did not allow the authors to follow the time course of the reactions. As a consequence, no transient states could be observed. This problem was partially solved by comparing and subtracting difference spectra of different reaction steps obtained for particularly conditioned samples. Difference spectra of phosphoenzyme conversion and the phosphorylation reaction could thus be obtained (8). However, this approach did not allow us to detect reaction intermediates, and the normalization procedure needed to compare different samples limits the reliability of these difference spectra. In addition, the spectrum of the phosphorylation reaction was obtained by subtracting a spectrum of $\text{Ca}_2\text{E}_1\cdot\text{ADP}$ from a spectrum of $\text{Ca}_2\text{E}_1\cdot\text{P}\cdot\text{ATP}$, and therefore reflects not only the reaction of interest (ATPase phosphorylation) but also the effects of binding of ATP's γ -phosphate to the ATPase. These limitations of steady-state infrared spectroscopy can be overcome by time-resolved infrared spectroscopy. This approach also avoids the intrinsic disadvantage of using caged compounds in infrared spectroscopy, *i.e.* the overlap of the absorbance changes of interest by absorbance changes due to the release of the effector molecule from the caged compound. Since the release reaction is fast compared with the ATPase reactions of phosphorylation and phosphoenzyme conversion, its contribution to the spectra can be separated.

Rapid scan FTIR spectroscopy allows one to collect the spectral data within milliseconds. This makes it possible to follow in real time the formation and decay of intermediates in the ATPase reaction cycle. There are three advantages of time-resolved infrared spectroscopy compared with other common methods for the kinetic investigation of the Ca^{2+} -ATPase reactions, which rely on the detection of radioactive Ca^{2+} or phosphate bound to the protein or on fluorescence measurements.

(i) Infrared spectroscopy is non-invasive, *i.e.* there is no need to label the protein; therefore, possible perturbations of protein structure due to the artificially introduced label are avoided.

(ii) The observation is not restricted to a limited number of chromophores (*i.e.* Trp residues) or to an extrinsic fluorescence label, which will largely reflect local changes in the vicinity of the chromophore(s) and may miss conformational changes occurring in distant regions of the protein. Instead, in infrared spectroscopy all carbonyl "chromophores" of the backbone amide groups are monitored, and this will reveal any change in backbone conformation even if very small.

(iii) In the same experiment it is possible to follow the kinetics of an overall conformational change of the polypeptide backbone, as well as the fate of single protein groups directly involved in a catalytic reaction. Thus infrared spectroscopy simultaneously looks, on the one hand, at highly specific local sites and, on the other hand, at the protein as a whole. As reactions at local sites we may consider here the formation of the aspartylphosphate group, dissociation of the complex between Ca^{2+} and the chelating protein groups, and changes of interaction to the phosphate group that are associated with the conversion from the ADP-sensitive to the ADP-insensitive phosphoenzyme.

In this work we report time-resolved changes in the infrared spectrum of the ATPase that occur after ATP release. For the first time the contributions to the infrared difference spectra of ATP binding, ATPase phosphorylation, and phosphoenzyme conversion could clearly be separated in the time domain. For the phosphorylation reaction and phosphoenzyme conversion reaction, infrared absorbance changes were monitored at time intervals of 65 ms and were evaluated in order to analyze the number of intermediates in the reaction. We are especially

interested in the following questions. (i) Do all local reactions associated with a particular reaction step proceed at the same time? (ii) Is it possible to reveal the triggering step of a partial reaction, *i.e.* does the protein change its conformation first before a local reaction can take place or, in contrast, do local reactions trigger and precede an overall change of protein conformation? In particular, is there a conformational change after $\text{Ca}_2\text{E}_1\cdot\text{P}$ formation but before Ca^{2+} release that may orient the Ca^{2+} binding sites toward the SR lumen?

MATERIALS AND METHODS

Sample Preparation— Ca^{2+} -ATPase prepared according to Ref. 11 was a generous gift of W. Hasselbach (Max-Planck-Institut, Heidelberg, Germany). Infrared samples were prepared as described previously (12). Briefly, after overnight dialysis in H_2O or $^2\text{H}_2\text{O}$ buffer, 10 μl of SR suspension plus appropriate additives to give the final sample composition (see Table I) were dried onto a CaF_2 window with a trough of 8 μm depth and 8 mm diameter. They were then rehydrated with approximately 0.6 μl of solvent (H_2O or $^2\text{H}_2\text{O}$ containing 0 or 20% Me_2SO). The sample was sealed with a second flat CaF_2 window and was thermostated at 1 $^\circ\text{C}$ during the experiment. The composition of the samples, which is specified in Table I, was designed to accumulate the $\text{Ca}_2\text{E}_1\cdot\text{P}$ state in samples termed *type I samples* and the $\text{E}_2\cdot\text{P}$ state in samples termed *type II samples*.

Two kinds of control samples were prepared. One contained caged AMP-PNP instead of caged ATP; the other was prepared without ATPase, but otherwise had the same sample composition as the type I and the type II samples.

Caged AMP-PNP was synthesized as described in Ref. 13 for caged ATP using AMP-PNP from Boehringer (Mannheim, Germany) as the starting material.

FTIR Measurements—FTIR measurements were performed with a modified Bruker IFS 66 spectrometer equipped with a HgCdTe detector of selected sensitivity. Data were acquired with double sided interferograms in a forward-backward mode at a spectral resolution of 4 cm^{-1} with the Blackman-Harris 4-term apodization function. The time needed for one interferometer cycle was 65 ms. The experiment started with the recording of spectra coadded from 300, 40, 4, and 1 scan (to check the signal to noise ratio and base-line stability) and a reference spectrum coadded from 300 scans characterizing the unperturbed sample. The time was set to zero, and photolysis of caged ATP was triggered with a xenon flash tube (12). The voltage of the flash power supply was set to release approximately 2–3 mM ATP/flash. Subsequently 10 spectra at 1 scan each, 10 spectra at 4 scans each, 10 spectra at 40 scans each, and 10 spectra at 300 scans each were recorded. After completion of the experiment done with one flash, the sample was allowed to equilibrate for at least 30 min at room temperature before the next flash was applied. Up to six flashes were applied to one sample. Spectra obtained from the average of several flashes did not differ significantly from spectra obtained from only the first flash. The spectra were normalized according to the protein content using the amide I or amide II absorbance as described in Ref. 12.

Calculation of Difference Spectra—The difference spectra were calculated as indicated in Fig. 2 (sample and reference spectra are labeled (+) and (–), respectively). The kinetic FTIR experiment produced difference spectra calculated with respect to the reference spectrum recorded before the flash, *i.e.* the absorbance of the ATPase states evolving after ATP release minus the absorbance of Ca_2E_1 . At appropriate times after ATP release, they thus represent the absorbance changes associated with ATP binding ($\text{Ca}_2\text{E}_1 \rightarrow \text{Ca}_2\text{E}_1\cdot\text{ATP}$), $\text{Ca}_2\text{E}_1\cdot\text{P}$ formation ($\text{Ca}_2\text{E}_1 \rightarrow \text{Ca}_2\text{E}_1\cdot\text{P}\cdot\text{ATP}$) and $\text{E}_2\cdot\text{P}$ formation ($\text{Ca}_2\text{E}_1 \rightarrow \text{E}_2\cdot\text{P}\cdot\text{ATP}$). Spectra calculated in this way, *i.e.* with the reference spectrum recorded before the flash, are abbreviated ΔA with the time interval of recording indicated in brackets, for example $\Delta A(71\text{--}385 \text{ ms})$ for the *ATP binding spectrum*. These spectra also show absorbance changes due to the photolysis reaction.

The *phosphorylation spectrum* of type I samples shows absorbance changes due to the reaction $\text{Ca}_2\text{E}_1\cdot\text{ATP} \rightarrow \text{Ca}_2\text{E}_1\cdot\text{P}\cdot\text{ATP}$. It was calculated by subtracting the absorbance of $\text{Ca}_2\text{E}_1\cdot\text{ATP}$ ($\Delta A(71\text{--}385 \text{ ms})$) from the absorbance of $\text{Ca}_2\text{E}_1\cdot\text{P}\cdot\text{ATP}$ ($\Delta A(3.25\text{--}11.0 \text{ s})$). An analogous spectrum was calculated in order to obtain the phosphorylation spectrum for the type II samples; however, the simple subtraction $\Delta A(3.25\text{--}11.0 \text{ s})$ minus $\Delta A(71\text{--}385 \text{ ms})$ resulted in a spectrum showing absorbance changes not only due to the phosphorylation reaction, but also due to the phosphoenzyme conversion reaction, which had already begun. The latter absorbance changes had to be eliminated. For this, a fraction

TABLE I
Approximate concentrations of ATPase and other constituents in the ATPase samples

Concentrations are based on a 1- μl sample volume and 4.5 nmol of active ATPase/mg of protein (19–25). The true sample volume varied between 0.6 and 1.2 μl . Mops, 4-morpholinepropanesulfonic acid.

Sample name	ATPase	Buffer	pH	K ⁺	Ca ²⁺	Glutathione	Caged ATP	ATP released	A23187	Adenylate kinase	Me ₂ SO
	<i>mM</i>			<i>mM</i>	<i>mM</i>	<i>mM</i>	<i>mM</i>	<i>mM</i>	<i>mg/ml</i>	<i>mg/ml</i>	%
Type I sample	0.7	300 mM Mops	7.0	330	10	20	20	2–3	0.5	2	0
Type II sample	0.7	300 mM imidazole	7.0	0	1	20	20	2–3	0.5	2	20

of the conversion spectrum (described below) was subtracted to obtain the “pure” phosphorylation spectrum. The criterion for a correct subtraction was a flat base line above 1730 cm^{-1} so that the band at 1758 cm^{-1} , which is characteristic for the phosphoenzyme conversion reaction (Fig. 4d and Ref. 8) did not appear in the phosphorylation spectrum.

The phosphoenzyme conversion spectrum monitors absorbance changes due to the reaction $\text{Ca}_2\text{E}_1\text{-P-ATP} \rightarrow \text{E}_2\text{-P-ATP}$. For its calculation a spectrum after $\text{Ca}_2\text{E}_1\text{-P}$ formation, $\Delta A(3.25\text{--}11.0\text{ s})$, was subtracted from $\Delta A(87.6\text{--}146\text{ s})$ after completion of $\text{E}_2\text{-P}$ formation. Since part of the conversion reaction had already proceeded before the selected time interval, this spectrum was normalized to give the full extent of the conversion spectrum using the bands at 1758 and 1570 cm^{-1} . They are characteristic for the $\text{E}_2\text{-P}$ state and are not overlapped by bands of the phosphorylation reaction (see Fig. 4, c and d). The normalization was done with respect to the amplitude of these bands in the spectrum of $\text{E}_2\text{-P}$ formation ($\text{Ca}_2\text{E}_1 \rightarrow \text{E}_2\text{-P-ATP}$, $\Delta A(87.6\text{--}146\text{ s})$; Fig. 4a).

For the spectra of control samples, the same time intervals were evaluated as for the phosphorylation and conversion reaction if not stated otherwise.

Fitting Procedures—For fitting of selected infrared absorbance changes to a kinetic model, we used integrated band intensities. Integration was performed with respect to a base line that was drawn between two data points of the spectrum at each side of the band. If necessary, special care was taken to generate integration boundaries leading to an integrated area characteristic for only one band out of a complex difference profile. This was used to separate the contributions of phosphorylation from those of phosphoenzyme conversion and to avoid overlap with bands that appeared in the control spectra. For example if the band of interest was disturbed by an overlaid difference profile consisting of a minimum and an adjacent maximum, the integration was carried out from the superimposed minimum to the maximum. In this way the base line for the integration connects the superimposed minimum and maximum and therefore follows closely the contour of the superimposed difference profile. This keeps the area between base line and superimposed difference profile to a small value. Moreover, negative and positive contributions are expected to cancel nearly completely. As a consequence, the integral is dominated by the band of interest with only a minor contribution from the overlaid band profile.

Fitting was done with the program “Mexfit” written by K. H. Müller (Max-Planck-Institut für molekulare Physiologie, Dortmund, Germany) and auxiliary software written by S. Gryzbek in our laboratory. To determine the rate constant of a reaction, several selections of bands with a high signal to noise ratio were used, which generally comprised (i) a broad selection of bands with good signal to noise ratio, some of them however showing a small slow base-line shift; (ii) a selection of bands without slow base-line drift; and, additionally for type II samples, (iii) a selection of bands characteristic only of the phosphorylation reaction; and (iv) a selection of bands characteristic only for the conversion reaction.

For the kinetic analysis the time slots of spectra recording were represented by their average time. The data were fitted with one time constant for bands only characteristic for one partial reaction, with two time constants for bands characteristic for both reactions. An additional time constant was introduced when a slow base-line drift was superimposed onto the bands of interest. The time constants for one reaction obtained from the different selections of infrared bands were averaged to get the final time constant for the reaction. The error was set to include all fit results for the different band selections.

In order to achieve a better signal to noise ratio, signals of up to six consecutive ATP releases in one sample were averaged to obtain the kinetic constant for the phosphorylation reaction. Evaluating only the first ATP release did not lead to significantly different time constants. In contrast, for the conversion reaction in type II samples, only the first flash was evaluated since the time-constant for the averaged signals of

up to six consecutive ATP releases in H_2O was nearly 30% larger. This effect was not found in $^2\text{H}_2\text{O}$; however, the fit results of different data sets vary more when all flashes are evaluated than upon evaluation of only the first ATP release.

The same programs were also used to fit the whole set of time-dependent difference spectra in order to calculate difference spectra that correlate to the time constants of the reaction. These spectra showed a slightly lower signal to noise ratio than spectra obtained by direct subtraction (described above). Both types of spectra showed good agreement. Therefore the difference spectra resulting from the fit were only used as a control for the more directly obtained spectra.

RESULTS

Infrared Absorbance Changes—ATP release from an inactive but photolabile precursor in ATPase samples leads to infrared absorbance changes evolving with time. In spite of their small amplitude, we were able to measure them precisely and to follow their time course. The changes are represented here in the form of difference spectra, which were calculated according to the scheme shown in Fig. 2. Negative and positive bands in a difference spectrum are due to molecular groups that change their structure or their interaction with the local environment in the course of the reaction, negative bands being characteristic for the initial state, positive bands for the intermediate or final state. The initial time resolution of the ATPase-associated absorption changes is limited owing to the ATP release reaction from caged ATP, which is complete only in the second spectrum recorded 71–126 ms after the photolysis flash. We have used two different sample compositions (see Table I) to accumulate the $\text{Ca}_2\text{E}_1\text{-P}$ state in type I samples and the $\text{E}_2\text{-P}$ state in type II samples.

Infrared Difference Spectra of Type I Samples—Fig. 3 shows infrared absorbance changes due to ATP release in type I samples, which contain no Mg^{2+} but 10 mM CaCl_2 and 330 mM KCl. These conditions were chosen to block the $\text{Ca}_2\text{E}_1\text{-P} \rightarrow \text{E}_2\text{-P}$ transition in order to achieve a maximum level of $\text{Ca}_2\text{E}_1\text{-P}$ in the steady state after ATP release while slowing down the phosphorylation reaction. Replacement of Mg^{2+} at the catalytic site by Ca^{2+} decreases the rate of phosphorylation by 1 order of magnitude (14–16). The high Ca^{2+} concentration (17) and the presence of K^+ (14, 15, 18) in our samples ensure that the accumulating phosphoenzyme is ADP-sensitive ($\text{Ca}_2\text{E}_1\text{-P}$).

The phosphoenzyme may accumulate to less than 100% of active ATPase molecules (4–5 nmol of active ATPase/mg of protein; Refs. 19–25) after ATP addition owing to the use of Ca^{2+} instead of Mg^{2+} as the catalytic ion. This was observed (15) using a low Ca^{2+} concentration of 0.1 mM, which does not inhibit the decay of $\text{Ca}_2\text{E}_1\text{-P}$. Other studies (16, 18) using higher Ca^{2+} concentrations of 0.2–10 mM show that 90–100% of the active ATPase molecules become phosphorylated. In our previous report (8), we used both Mg^{2+} and Ca^{2+} as the catalytic ion. The band at 1719 cm^{-1} that appears upon ATPase phosphorylation (Fig. 3b, discussed below) showed the same intensity in both samples and in the samples of this work. We conclude that the replacement of Mg^{2+} by Ca^{2+} at the catalytic site does not significantly decrease the amount of phosphoenzyme in our samples.

The catalytic production of millimolar ADP concentrations in our highly concentrated ATPase samples may decrease the

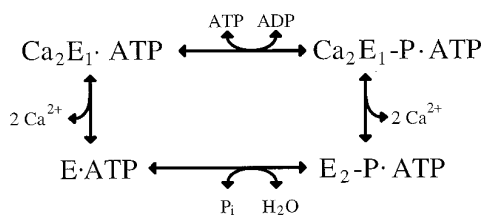


FIG. 1. Simplified scheme of the reaction cycle (2).

amount of $\text{Ca}_2\text{E}_1\text{-P}$ by favoring the back reaction from $\text{Ca}_2\text{E}_1\text{-P}$ to $\text{Ca}_2\text{E}_1\text{ATP}$ (26–29) (*upper step* in Fig. 1). These studies report a decrease to 35–70% of the maximum phosphoenzyme level at ADP concentrations in the millimolar range. However, according to the following considerations, ADP is unlikely to reduce the phosphoenzyme level in our samples.

(i) High Ca^{2+} concentrations in the millimolar range as in our samples inhibit the back reaction $\text{Ca}_2\text{E}_1\text{-P} \rightarrow \text{Ca}_2\text{E}_1$ catalyzed by ADP (18), thereby reducing the effect of ADP on the phosphoenzyme level. The effect was attributed to the formation of the Ca^{2+} complex of ADP, which is not the substrate for the back reaction (18).

(ii) Our samples contained a small amount of adenylate kinase, which removes the ADP produced. This is evident from the absorbance changes associated with the slow steady state hydrolysis of ATP (data not shown) observed after the ATPase is completely phosphorylated. A positive band appearing at 980 cm^{-1} indicates AMP and ATP production. This band is not present in samples without adenylate kinase (data not shown). Instead, a positive band near 950 cm^{-1} is observed, which is due to ADP production. Therefore adenylate kinase does remove the ADP produced. The following observations may indicate that ADP is not removed immediately and that it is transiently present. A small band near 940 cm^{-1} which appears upon ATPase phosphorylation may be assigned to the reaction product ADP. In the spectrum of slow steady state ATP hydrolysis, a negative shoulder at 930 cm^{-1} may be due to the consumption of ADP. Although these assignments are not unambiguous, the observations are in agreement with ADP being transiently present. If the ADP transiently present were to initially decrease the phosphoenzyme level, we would expect the bands formed during the initial phosphorylation reaction to increase further as ADP is removed. This is not observed within the time of the experiment (3.5 min).

(iii) The ATPase concentration used in the studies cited above was at least 100 times lower than in our infrared samples. A high concentration of the two cation-binding proteins calbindin and calmodulin was reported to reduce their cation binding affinity and was explained by the general phenomenon of electrostatic screening (30). Therefore it is possible that the affinity of $\text{Ca}_2\text{E}_1\text{-P}$ for ADP is reduced in the infrared samples as compared with diluted samples.

In conclusion, the phosphoenzyme level in our samples does not seem to be drastically reduced by ADP. We have to assume that the phosphoenzyme binds ATP under our conditions of high (greater than millimolar) ATP concentrations (2) (for evidence in the spectra see “Discussion”). Therefore we attribute the infrared signals shown in Fig. 3 to the reaction $\text{Ca}_2\text{E}_1 \rightarrow \text{Ca}_2\text{E}_1\text{-P}\cdot\text{ATP}$.

Fig. 3a shows two difference spectra representing an intermediate and the final stage of this reaction, $\Delta A(71\text{--}385\text{ ms})$ (*solid line*) and $\Delta A(3.25\text{--}11.0\text{ s})$ (*dotted line*). They were calculated from spectra recorded at the indicated time intervals after the photolysis flash and a reference spectrum before the flash (see Fig. 2 for a scheme of spectra calculation). In addition to absorbance changes due to the ATPase reaction, they also show changes due to the photolysis reaction, *i.e.* the band at

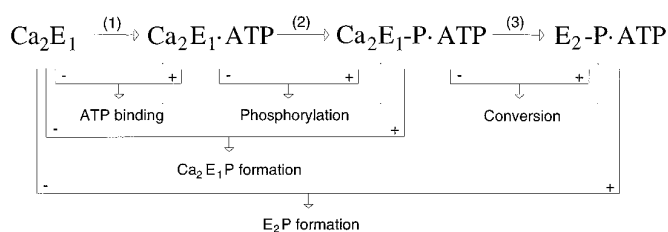


FIG. 2. Reaction steps investigated in this study. The lower part of the scheme illustrates the calculation of difference spectra. Spectra of connected enzyme states were subtracted; + and – refer to the sign of the spectrum in the calculation.

1529 cm^{-1} as well as the dominating bands below 1350 cm^{-1} (for a discussion of the photolysis difference spectrum, see Refs. 12 and 31).

The first spectrum, $\Delta A(71\text{--}385\text{ ms})$ (*solid line*), shows major bands in the 1700–1600 cm^{-1} region and between 1500 and 1380 cm^{-1} , which cannot be attributed to the photolysis reaction. Because of the striking agreement with the difference spectrum (32) after release of AMP-PNP, a non-hydrolyzable ATP analogue, these changes are attributed to the ATP binding reaction $\text{Ca}_2\text{E}_1 \rightarrow \text{Ca}_2\text{E}_1\text{ATP}$ and the *solid line* spectrum in Fig. 3a is therefore termed *ATP binding spectrum*.

Small changes are observed afterward, which are most clearly seen in Fig. 3a above 1700 cm^{-1} and near 1553 cm^{-1} . After 3 s the steady state is reached in which the $\text{Ca}_2\text{E}_1\text{-P}$ state accumulates. Thus the *dotted spectrum* in Fig. 3a, $\Delta A(3.25\text{--}11.0\text{ s})$, represents the reaction $\text{Ca}_2\text{E}_1 \rightarrow \text{Ca}_2\text{E}_1\text{-P}\cdot\text{ATP}$ and is therefore termed the *Ca₂E₁ → Ca₂E₁-P spectrum*.

As already mentioned above, a regulatory ATP molecule is expected to bind to the phosphoenzyme. In our spectra in Fig. 3a, it is obvious that bands which can be attributed to ATP binding (*solid line*) are still present in the late spectrum after complete $\text{Ca}_2\text{E}_1\text{-P}$ formation (*dotted line*), *i.e.* bands at 1663, 1641, 1627, and 1477 to 1402 cm^{-1} , indicating that a nucleotide is still bound to the phosphoenzyme. The possibility that a regulatory ATP molecule but not the reaction product ADP binds to the phosphoenzyme can be rationalized for the following reasons. (i) It is known that millimolar ATP concentrations accelerate all major steps of the reaction at low ATPase concentration (typically less than 1 mg/ml) (2, 33). (ii) The spectra of ADP (8) and ATP binding (this work) differ particularly near 1620 cm^{-1} at the low wavenumber side of the 1627 cm^{-1} band, where the amplitude is higher for ATP. Thus, if ADP were to bind to the phosphoenzyme, we should observe a decrease in absorption at approximately 1620 cm^{-1} in the reaction from $\text{Ca}_2\text{E}_1\cdot\text{ATP}$ to the phosphoenzyme. This is not observed. Considering these arguments, we conclude that ATP is bound to $\text{Ca}_2\text{E}_1\text{-P}$ in the type I samples.

Fig. 3b shows absorbance changes after ATP binding, which take place between 400 ms and 3 s after photolysis. The spectra were calculated by subtracting the ATP binding spectrum from the spectra of $\text{Ca}_2\text{E}_1\text{-P}$ formation, thus showing the effects of the phosphorylation reaction $\text{Ca}_2\text{E}_1\cdot\text{ATP} \rightarrow \text{Ca}_2\text{E}_1\text{-P}\cdot\text{ATP}$. After 3 s the reaction is complete and the corresponding difference spectrum is subsequently termed the *phosphorylation spectrum* (*solid line* in Fig. 3b). A spectrum at an earlier stage of the time course is shown as the *dotted line* in Fig. 3b. Neither spectrum shows bands due to the photolysis reaction since these cancel in the subtraction.

The band at 1719 cm^{-1} in Fig. 3b showing formation of a C=O group was tentatively attributed to the phosphorylated Asp^{351} (8). However, owing to the steady state approach of this study (8), it was in principle possible that the band was caused by the binding of ATP's γ -phosphate and not the phosphorylation reaction. The kinetic approach used here shows unambig-

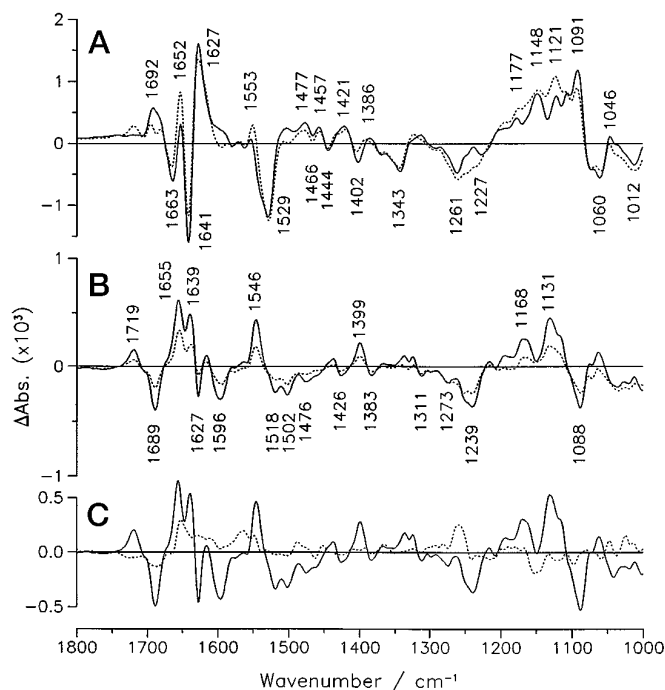


FIG. 3. Infrared difference spectra upon ATP release in type I samples in H_2O (1 °C, pH 7.0). Average of a total of 26 ATP releases in six different samples. Labels refer to the *solid line* spectra. *a*, spectra of ATP binding (*solid line*, $\text{Ca}_2\text{E}_1 \rightarrow \text{Ca}_2\text{E}_1\text{-ATP}$, $\Delta A(71\text{--}385\text{ ms})$) and of $\text{Ca}_2\text{E}_1\text{-P}$ formation (*dotted line*, $\text{Ca}_2\text{E}_1 \rightarrow \text{Ca}_2\text{E}_1\text{-P-ATP}$, $\Delta A(3.25\text{--}11.0\text{ s})$), both showing infrared bands due to the photolysis reaction. *b*, difference spectra of the phosphorylation reaction ($\text{Ca}_2\text{E}_1\text{ATP} \rightarrow \text{Ca}_2\text{E}_1\text{-P-ATP}$) at different time intervals. *Solid line*, phosphorylation spectrum $\Delta A(3.25\text{--}11.0\text{ s})$ minus $\Delta A(71\text{--}385\text{ ms})$; *dotted line*, $\Delta A(655\text{--}1423\text{ ms})$ minus $\Delta A(71\text{--}385\text{ ms})$. *c*, comparison between the phosphorylation spectrum (*solid line*) and the control spectrum after release of AMP-PNP (*dotted line*).

uously that the formation of the 1719 cm^{-1} band is due to the phosphorylation reaction.

The same phosphorylation spectrum was obtained in samples containing only 3 mM CaCl_2 , but the amplitudes relative to those of the ATP binding spectrum were smaller than for the samples containing 10 mM CaCl_2 . We think that this is due to a smaller extent of inhibition of the phosphoenzyme conversion step leading to a smaller $\text{Ca}_2\text{E}_1\text{-P}$ concentration in the steady state of the low Ca^{2+} samples.

Control Spectra—Two kinds of control samples were used to check the effect of side reactions of the photolysis by-products on the infrared difference spectra. Side reactions are expected in the presence of the reducing agent glutathione. In one kind of control experiment, caged ATP was released in samples containing no ATPase but otherwise of a composition identical to the type I samples. In the other kind of control experiment AMP-PNP instead of ATP was released from caged AMP-PNP in ATPase containing samples. A difference spectrum of the latter samples obtained in the same time interval as the phosphorylation spectrum is shown as a *dotted line* in Fig. 3c. Generally, the absorbance changes of this control spectrum are very small ($<0.2 \cdot 10^{-3}$), and in most spectral regions the phosphorylation spectrum is only slightly affected by side reactions. However, some of the control signals are comparable in their amplitude to those of the phosphorylation spectrum (near 1655, 1260, and 1150 cm^{-1}). Therefore special attention was paid when evaluating the kinetic signals of the phosphorylation reaction in order to minimize the effect of possibly overlapping bands of side reactions (see “Materials and Methods”). The bands of the control spectrum are also observed upon caged ATP photolysis in ATPase-free samples and can therefore be

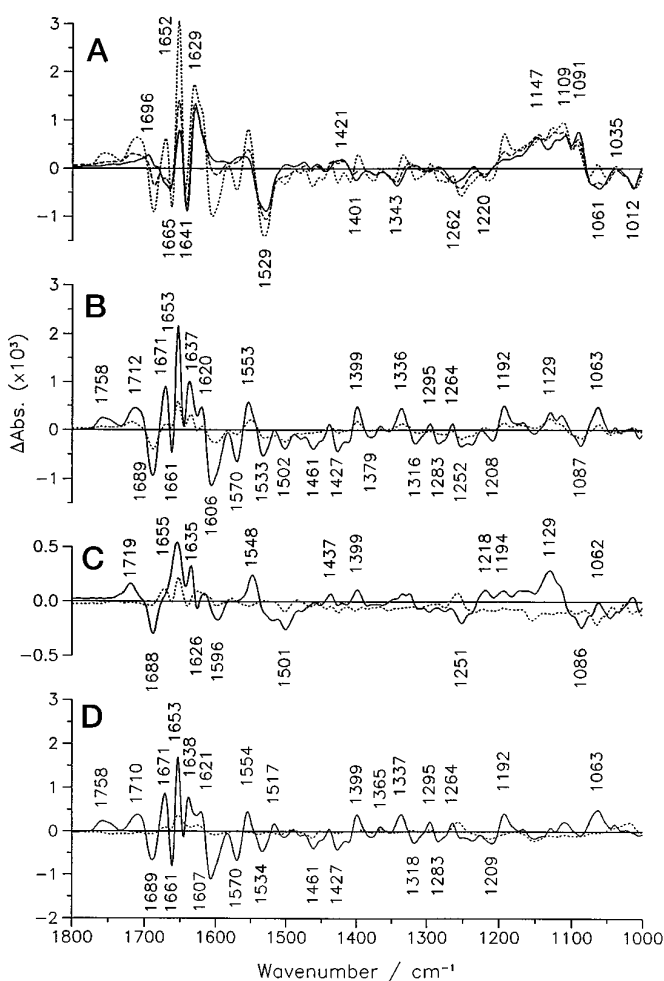


FIG. 4. Infrared difference spectra upon ATP release in type II samples in H_2O (1 °C, pH 7.0). Average of a total of 28 ATP releases in seven different samples. Labels refer to the *solid line* spectra. *a*, spectra of ATP binding (*solid line*, $\text{Ca}_2\text{E}_1 \rightarrow \text{Ca}_2\text{E}_1\text{-ATP}$, $\Delta A(71\text{--}385\text{ ms})$), predominantly $\text{Ca}_2\text{E}_1\text{-P}$ formation (*dashed line*, $\text{Ca}_2\text{E}_1 \rightarrow \text{Ca}_2\text{E}_1\text{-P-ATP}$, $\Delta A(2.21\text{--}3.24\text{ s})$) and $\text{E}_2\text{-P}$ formation (*dotted line*, $\text{Ca}_2\text{E}_1 \rightarrow \text{E}_2\text{-P-ATP}$, $\Delta A(87.6\text{--}145.9\text{ s})$), all also showing infrared bands due to the photolysis reaction. *b*, Same as in *a*, but the ATP binding spectrum is subtracted from the spectra of $\text{Ca}_2\text{E}_1\text{-P}$ formation and $\text{E}_2\text{-P}$ formation, therefore representing the reactions of predominantly $\text{Ca}_2\text{E}_1\text{ATP} \rightarrow \text{Ca}_2\text{E}_1\text{-P-ATP}$ (*dotted line*) and $\text{Ca}_2\text{E}_1\text{ATP} \rightarrow \text{E}_2\text{-P-ATP}$ (*solid line*). *c*, comparison between phosphorylation spectrum (*solid line*, $\text{Ca}_2\text{E}_1\text{ATP} \rightarrow \text{Ca}_2\text{E}_1\text{-P-ATP}$) and control spectrum after release of AMP-PNP (*dotted line*). The phosphorylation spectrum was calculated by subtracting from $\Delta A(3.25\text{--}11.02\text{ s})$ the ATP binding spectrum $\Delta A(71\text{--}385\text{ ms})$ and absorbance changes due to already formed $\text{E}_2\text{-P-ATP}$ as described under “Materials and Methods.” For the control spectrum $\Delta A(3.25\text{--}11.0\text{ s})$ and $\Delta A(71\text{--}645\text{ ms})$ were subtracted. *d*, comparison between the conversion spectrum (*solid line*, $\text{Ca}_2\text{E}_1\text{-P-ATP} \rightarrow \text{E}_2\text{-P-ATP}$, normalized $\Delta A(87.6\text{--}146\text{ s})$ minus $\Delta A(3.25\text{--}11.0\text{ s})$) as described under “Materials and Methods”) and the control spectrum after release of AMP-PNP (*dotted line*), calculated from spectra obtained in the same time intervals and multiplied with the same normalization factor.

attributed to a slow reaction following caged ATP photolysis, which most likely involves the photolysis by-product nitrosoacetophenone. A detailed study of these reactions is currently under way.

Infrared Difference Spectra of Type II Samples—Fig. 4 shows spectra obtained with type II samples. Owing to the addition of 20% Me_2SO and the omission of K^+ , the ADP-insensitive phosphoenzyme intermediate $\text{E}_2\text{-P}$ is expected to accumulate in these samples (25, 34). In contrast to our previous experiments (8), these samples contained 1 mM Ca^{2+} instead of 15 mM Mg^{2+} , which may have an influence on the amount of $\text{E}_2\text{-P}$ accumulating. To address this point, the two bands at 1192 and 1758

cm^{-1} known to be characteristic for the $E_2\text{-P}$ state (8) (see also Fig. 4, *a* and *d*) were taken as markers for $E_2\text{-P}$ and their amplitudes investigated under varying conditions. The replacement of Mg^{2+} by Ca^{2+} did not change the amplitudes of these marker bands in the presence of 20% Me_2SO , indicating that the accumulation of $E_2\text{-P}$ is not perturbed by the presence of Ca^{2+} in our samples. The omission of Me_2SO leads to a significant reduction of the marker band intensities even under otherwise optimal conditions for $E_2\text{-P}$ accumulation (15 mM Mg^{2+} , no K^+), the decrease being even more drastic when Mg^{2+} was replaced by 2 mM Ca^{2+} . This corresponds to the finding of only 20–40% of the phosphoenzyme in the $E_2\text{-P}$ form in the presence of Ca^{2+} and the absence of K^+ , Mg^{2+} , and Me_2SO (15, 16, 18). In our type II samples, however, as demonstrated by the $E_2\text{-P}$ marker bands, the presence of 20% Me_2SO ensures the accumulation of the $E_2\text{-P}$ state. As already discussed for $\text{Ca}_2E_1\text{-P}$, a regulatory ATP molecule is expected to bind to the phosphoenzyme (for the discussion of the effects of ATP binding on the spectra, see below).

Fig. 4*a* shows absorbance changes occurring in the time course of the reaction $\text{Ca}_2E_1 \rightarrow E_2\text{-P}\cdot\text{ATP}$, taken at different time ranges after photolysis (*solid line*, $\Delta A(71\text{--}385\text{ ms})$; *dashed line*, $\Delta A(2.21\text{--}3.24\text{ s})$; *dotted line*, $\Delta A(87.6\text{--}146\text{ s})$). The spectra reveal two reaction intermediates (*solid line* and *dashed line*) before $E_2\text{-P}\cdot\text{ATP}$ is finally formed (*dotted line*). They also show absorbance changes due to the photolysis reaction (band at 1529 cm^{-1} and the dominating bands below 1350 cm^{-1}). Owing to the similarity of the early spectrum (*solid line*) to a difference spectrum obtained after release of the ATP analogue AMP-PNP (data not shown), we attribute the early spectrum to ATP binding to the ATPase and call it the ATP binding spectrum. The *dashed line* spectrum represents a second intermediate in the reaction and not just partially formed $E_2\text{-P}\cdot\text{ATP}$ because it is different from the final spectrum of $E_2\text{-P}\cdot\text{ATP}$ formation. This is most evident from the band above 1700 cm^{-1} , which has a different position in the spectrum of the second intermediate (*dashed line*, 1719 cm^{-1}) from that in the late spectrum (*dotted line*, 1710 cm^{-1}). In addition, fast and slow kinetics of bands can be detected already by visual inspection; The band at 1689 cm^{-1} has evolved to nearly half of its maximal amplitude in the second intermediate spectrum (*dashed line*), whereas other bands have evolved to a much lesser extent at that time (see for example bands at 1758 , 1671 , 1606 , and 1192 cm^{-1} ; these bands are labeled in Fig. 4*b*). This second intermediate will be shown to be $\text{Ca}_2E_1\text{-P}$ when discussing Fig. 4*c*. Therefore, the *dashed line* intermediate spectrum is attributed to formation of mainly $\text{Ca}_2E_1\text{-P}\cdot\text{ATP}$ with a small contribution of already formed $E_2\text{-P}\cdot\text{ATP}$.

A regulatory ATP molecule is still bound to the enzyme in the $E_2\text{-P}$ state. This is evident at 1641 and 1629 cm^{-1} , where ATP binding bands are still observed after $E_2\text{-P}$ formation has finished (*dotted spectrum*).

Fig. 4*b* shows absorbance changes after ATP binding is complete. They correspond to an intermediate and the final stage of the reaction $\text{Ca}_2E_1\text{-ATP} \rightarrow E_2\text{-P}\cdot\text{ATP}$. The intermediate spectrum is dominated by bands due to the phosphorylation reaction ($\text{Ca}_2E_1\text{-ATP} \rightarrow \text{Ca}_2E_1\text{-P}\cdot\text{ATP}$), whereas the late spectrum shows the effects of both phosphorylation and phosphoenzyme conversion ($\text{Ca}_2E_1\text{-ATP} \rightarrow E_2\text{-P}\cdot\text{ATP}$). The two phosphoenzymes are again discernible at the two bands mentioned above.

The *solid line* spectrum shown in Fig. 4*c* allows the identification of the intermediate in the reaction from $\text{Ca}_2E_1\text{-ATP}$ to $E_2\text{-P}\cdot\text{ATP}$. The spectrum corresponds to the absorbance at an intermediate time interval after photolysis (3.25–11.0 s) minus the absorbance of the ATP bound state $\text{Ca}_2E_1\text{-ATP}$ with a correction to cancel the absorbance changes due to already

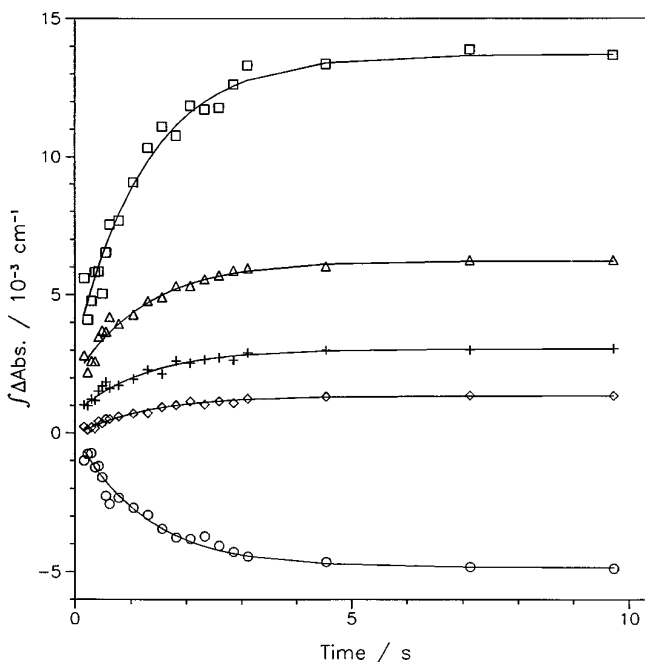


FIG. 5. Kinetics of selected infrared bands of type I samples (1 °C, pH 7.0). Labels refer to the wavenumber of absorption in cm^{-1} . Different constants were added to each kinetic trace to obtain a clear presentation. +, 1719; \circ , 1689; \triangle , 1546; \diamond , 1399; \square , 1131.

formed $E_2\text{-P}\cdot\text{ATP}$ (see “Materials and Methods”). Thus it shows only absorbance changes due to the reaction from $\text{Ca}_2E_1\text{-ATP}$ to the intermediate state. This spectrum is in very good agreement with the phosphorylation spectrum of type I samples shown in Fig. 3*b*. We take this argument as evidence for the attribution of the *solid line* spectrum in Fig. 4*c* to the phosphorylation reaction $\text{Ca}_2E_1\text{-ATP} \rightarrow \text{Ca}_2E_1\text{-P}\cdot\text{ATP}$ and term it the phosphorylation spectrum. In conclusion, one intermediate in the reaction from $\text{Ca}_2E_1\text{-ATP}$ to $E_2\text{-P}\cdot\text{ATP}$ was found and identified to be $\text{Ca}_2E_1\text{-P}\cdot\text{ATP}$.

The *dotted line* in Fig. 4*c* shows the control spectrum recorded after release and binding of AMP-PNP to the ATPase to investigate possible absorbance changes that are not associated with phosphorylation, for example due to side reactions of the photolysis by-product with glutathione. A comparison with the *solid line* spectrum shows that most phosphorylation bands are hardly affected by the side reactions, whereas some bands will have a side reaction contribution (1655 and 1251 cm^{-1}) and one band can be attributed to the side reaction (1501 cm^{-1}).

The *solid line* of Fig. 4*d* shows a difference spectrum of the late events of $E_2\text{-P}\cdot\text{ATP}$ formation after complete $\text{Ca}_2E_1\text{-P}\cdot\text{ATP}$ formation ($\Delta A(87.6\text{--}145.9\text{ s}) - \Delta A(3.25\text{--}11.02\text{ s})$), *i.e.* absorbance changes due to phosphoenzyme conversion $\text{Ca}_2E_1\text{-P}\cdot\text{ATP} \rightarrow E_2\text{-P}\cdot\text{ATP}$. This spectrum was normalized as described under “Materials and Methods” and is termed the conversion spectrum. It is in good agreement with the conversion spectrum shown in Fig. 8 of Ref. 8, which was obtained in a much more indirect way by comparing normalized difference spectra of different samples in different buffers. The *dashed line* of Fig. 4*d* shows the control spectrum for type I samples after AMP-PNP release. Owing to the larger amplitude of the conversion signals, the conversion spectrum is much less affected by side reactions than the phosphorylation spectrum.

Time Constants of the Infrared Difference Bands—The time course of absorbance changes after ATP binding was analyzed. For type I samples, Fig. 5 shows the time course and the fit at selected wavenumbers which monitor changes in the absorption region of Asp and Glu side chain C=O modes (1719 cm^{-1}),

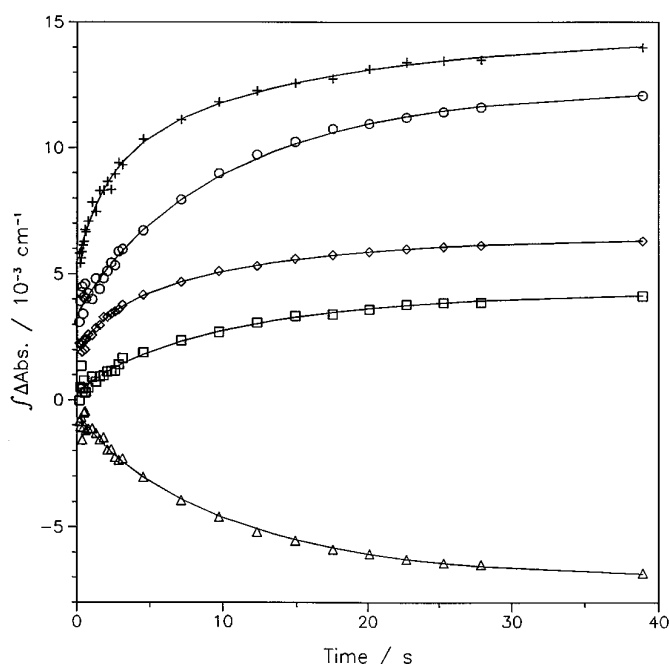


FIG. 6. Kinetics of selected infrared bands of type II samples (1 °C, pH 7.0). Labels refer to the wavenumber of absorption in cm^{-1} . Different constants were added to each kinetic trace to obtain a clear presentation. +, 1712; O, 1653; Δ , 1570; \diamond , 1399; \square , 1192.

of the amide I and II modes of the polypeptide backbone (1689 and 1546 cm^{-1} , respectively), of Asp and Glu carboxylate modes (1399 cm^{-1}), and of phosphate vibrations (1131 cm^{-1}). The signal at 1719 cm^{-1} was tentatively assigned to the formation of a C=O group in Asp³⁵¹ upon its phosphorylation (8). All signals in H_2O were fitted with a time constant of $1.27 \text{ s} \pm 15\%$ ($k_{\text{app}} = 0.79 \text{ s}^{-1}$, pH 7.0, 1 °C). In $^2\text{H}_2\text{O}$ the reaction was 1.5-fold slower than in H_2O with a time constant of $1.96 \text{ s} \pm 15\%$ ($k_{\text{app}} = 0.51 \text{ s}^{-1}$, p²H 7.0, 1 °C).

Fig. 6 shows the time course of absorbance changes at selected wavenumbers for type II samples comprising the absorption regions of protonated carboxyl groups of Asp and Glu side chains (1712 cm^{-1}), of the amide I vibration (1653 cm^{-1}), of Asp and Glu carboxylate groups (1570 and 1399 cm^{-1}), and of phosphate groups (1192 cm^{-1}). The signals above 1700 cm^{-1} were tentatively attributed to the protonation of carboxylate groups after Ca^{2+} release, the signals at 1570 and 1399 cm^{-1} to Ca^{2+} release from carboxylate groups (ν_{as} and ν_{s}) (8). It is evident that the time course observed needs to be analyzed with two time constants. The proportion of the signal occurring in the fast phase is largest at the 1712 cm^{-1} band. The fast reaction is associated with the phosphorylation reaction. In type II samples, phosphorylation seems to proceed slightly slower than in type I samples, the time constants being $1.44 \text{ s} \pm 15\%$ ($k_{\text{app}} = 0.69 \text{ s}^{-1}$) in H_2O and $2.63 \text{ s} \pm 10\%$ in $^2\text{H}_2\text{O}$ ($k_{\text{app}} = 0.38 \text{ s}^{-1}$, 1.8-fold slower than in H_2O).

These phosphorylation rates are in agreement with published values. In the presence of 0.2–10 mM Ca^{2+} , 100 mM KCl, and in the absence of Mg^{2+} at pH 7.0 and 0 °C, they vary between 0.1 and 0.6 s^{-1} (14, 15, 18). The lowest value (18) was obtained with $0.5 \mu\text{M}$ ATP, which is not saturating. Extrapolation of the ATP dependence (18) of the rate constant to saturating ATP concentrations leads to a rate constant twice as high as that observed at $0.5 \mu\text{M}$ ATP. At 5 °C in the absence of K^+ a value of 0.6 s^{-1} was found (16). A change in Ca^{2+} concentration from approximately 0.1 mM to 10 mM does not significantly affect the rate constant (14, 15, 18).

The slow time constant of type II samples is due to phos-

phoenzyme conversion and Ca^{2+} release. The associated time constants were found to be $10.9 \text{ s} \pm 7\%$ ($k_{\text{app}} = 0.092 \text{ s}^{-1}$, pH 7.0, 1 °C) in H_2O and $32.5 \text{ s} \pm 10\%$ in $^2\text{H}_2\text{O}$ ($k_{\text{app}} = 0.031 \text{ s}^{-1}$, 3-fold slower than in H_2O , p²H 7.0, 1 °C). The rate in H_2O is 4.5 times higher than the value of 0.020 s^{-1} reported in the literature (15) in the absence of Mg^{2+} and K^+ and the presence of 0.1 mM Ca^{2+} at 0 °C and pH 7.0. This value was estimated from the ratio between the rate of ATP hydrolysis and the level of ADP-sensitive phosphoenzyme. The discrepancy with our data may be due to the accelerating effect of high ATP concentrations, which is more pronounced in the absence of alkali ions (26) or to the presence of Me_2SO in our experiments. 20% Me_2SO was found to accelerate Ca^{2+} release from the phosphoenzyme by a factor of 4 at pH 7.0, 6 °C, 20 mM MgCl_2 , 300 mM KCl (35), whereas it has virtually no effect at pH 6.0, 20 °C, 20 mM MgCl_2 , no KCl (36).

Under all conditions ATP binding was complete within 130 ms after the photolysis flash. Afterward all significant infrared bands of the phosphorylation reaction could be fitted with only one time constant for type I samples. In analogy, bands due to the reaction $\text{Ca}_2\text{E}_1 \rightarrow \text{E}_2\text{-P}\cdot\text{ATP}$ of type II samples were successfully fitted with only two time constants, one for the phosphorylation reaction, the other for phosphoenzyme conversion and Ca^{2+} release. No additional long-lived intermediates were found.

DISCUSSION

Interpretation of the Kinetic Data—The partial reactions after ATP binding can be fitted with only two time constants associated with the consecutive formation of $\text{Ca}_2\text{E}_1\text{-P}$ and $\text{E}_2\text{-P}$. This finding does not support the assumption of additional long-lived intermediates in the ATPase reaction cycle, such as, for example, a Ca^{2+} -containing $\text{E}_2\text{-P}$ intermediate. This intermediate is part of the original model for the ATPase reaction cycle described by de Meis and Vianna (3). However, it is evident that fast reacting intermediates cannot be resolved with our method. For example, we could not resolve ADP release after ATPase phosphorylation from the binding of a regulatory ATP molecule.

Prior to phosphorylation, a rate-limiting conformational change in $\text{Ca}_2\text{E}_1\text{ATP}$ has been reported, which is followed by a fast phosphorylation reaction (5, 29). Since we observe only one time constant for the phosphorylation reaction, our phosphorylation spectra may represent both the conformational change of $\text{Ca}_2\text{E}_1\text{ATP}$ and the phosphorylation reaction.

The observation of only a single time constant for each reaction step is especially interesting in the light of infrared spectroscopy monitoring catalytic reactions at local sites in the protein, as well as the overall conformational change. The local effects we consider here are (i) the formation of the aspartylphosphate moiety, (ii) dissociation of the complex between Ca^{2+} and protein groups, and (iii) changes in the environment of the phosphate group connected with the transition of the phosphoenzyme from the state that is ADP-sensitive but stable against hydrolysis to the state that is ADP-insensitive but sensitive to hydrolytic attack. These reactions will be reflected in absorbance changes of the amino acid side chains and the phosphate group. The signal to noise ratio in the experiments presented here is good enough to detect absorbance changes of individual amino acids in the case of the Ca^{2+} -ATPase, a protein consisting of 1001 amino acids (37). For example, the positive band at 1719 cm^{-1} (Fig. 3) has been tentatively assigned to formation of a keto group upon aspartylphosphate formation (8).

In this context, a limited molecular interpretation is of interest. There are specific regions in the spectra in which the vibrational modes of the backbone amide groups absorb (amide

I mode, 1700–1610 cm^{-1} ; amide II mode, 1580–1500 cm^{-1}). The amino acid side chains and the bound nucleotide absorb in the entire observed spectral region from 1800 to 900 cm^{-1} , the transferred phosphate absorbs below 1300 cm^{-1} . Therefore, spectral regions outside the amide absorption provide the chance to observe the direct effects of local reactions without interference from signals due to a conformational change of the polypeptide backbone. On the other hand, in the regions of amide absorption, the backbone conformational changes will be observed. Thus, the restriction of absorption of specific groups to distinct spectral regions gives infrared spectroscopy the potential to discriminate between a reaction at a local site of the protein and the resulting or preceding overall conformational change. Our finding of only one time constant per partial reaction therefore leads to the conclusion that the local reactions proceed at the same time as the overall conformational change of the protein backbone. In particular, for the phosphoenzyme conversion reaction, we found that absorbance changes tentatively attributed to the effects of Ca^{2+} release (1758, 1712, 1570, and 1553 cm^{-1}) proceed at the same time as absorbance changes in the phosphate region of the spectrum. This indicates that there is no lag phase between the conversion of the phosphoenzyme from the ADP-sensitive to the ADP-insensitive form and Ca^{2+} release, and both processes occur in a concerted manner.

Kinetic Isotope Effect in $^2\text{H}_2\text{O}$ —The phosphorylation and the phosphoenzyme conversion reaction are slowed down in $^2\text{H}_2\text{O}$ by a factor of 1.5 or 3, respectively. A primary isotope effect, which is caused by X-H bond cleavage, is not likely to be the reason for the effect since it is expected to slow down the reaction by a factor between 6 and 8 (38). A kinetic isotope effect of 1.5, as observed for the phosphorylation reaction, is well within the range of secondary isotope effects due to a reorganization of vibrational energy levels of X-H vibrations in the course of the reaction (38). A kinetic isotope effect of 3, as observed for the $\text{Ca}_2\text{E}_1\text{-P} \rightarrow \text{E}_2\text{-P}$ conversion, is high for a secondary isotope effect but may be caused by cumulative effects of several groups.

A shifted pH dependence of the reaction in $^2\text{H}_2\text{O}$ may also contribute to the slowing down of phosphoenzyme conversion. This is due to H_3O^+ and OH^- being a stronger acid and base in $^2\text{H}_2\text{O}$ than in H_2O (38, 39) and therefore changing the dissociation equilibrium of acidic or basic protein residues. The rate of Ca^{2+} release from the phosphoenzyme is pH-dependent, increasing with increasing pH near pH 7.0 (35, 36). This pH dependence is likely to shift in $^2\text{H}_2\text{O}$. Assuming the titration of acidic groups to be responsible for the pH dependence, a shift of the titration curve to higher pH values is expected in $^2\text{H}_2\text{O}$ since the pK of acidic groups in $^2\text{H}_2\text{O}$ is typically 0.5 higher than in H_2O (39). Consequently, the rate of Ca^{2+} release would be slower in $^2\text{H}_2\text{O}$ than in H_2O . However, a typical shift most likely accounts for only part of the isotope effect, since the rate would be slowed down by only a factor of 1.3 (estimated from the pH dependence in Ref. 35). Other effects such as changes of hydrogen bonding may also contribute to the kinetic isotope effect. Kinetic isotope effects have been found previously for the beef heart mitochondrial ATPase (40, 41).

Change of Secondary Structure—The amide I mode of the polypeptide backbone, which is predominantly a C=O vibration, absorbs in the region from 1700 to 1610 cm^{-1} (42). The peak position of the amide I mode of a peptide group depends upon the secondary structure into which it is inserted. Analysis of amide I band components (for recent reviews, see Refs. 42–45) has been developed as an efficient tool for the analysis of the secondary structure of proteins. On this basis, the amplitude of the infrared difference signals in the amide I region

can be used to estimate the change of secondary structure. If we proceed along this line, we have to consider the following limitations.

(i) Signals of conformational changes may overlap in a way that they cancel each other leading to an underestimation of the extent of structural change. Therefore the infrared difference spectrum reveals only the *net* change of secondary structure.

(ii) Signals due to amino acid side chains may overlap, although the amide I mode has a strong extinction coefficient (46, 47), which is generally larger than that of amino acid side chains in the amide I region (48, 49).

(iii) In addition to a secondary structure change, more subtle changes such as changes of hydrogen bonding to the C=O oxygen within a persisting secondary structure will also manifest in the spectrum.

In order to quantify the structural changes of the polypeptide backbone in the ATPase partial reactions, we here introduce a *change of backbone structure and interaction (COBSI)* index. The calculation of the COBSI index for a difference spectrum of a partial reaction is carried out in the amide I region from 1700 to 1610 cm^{-1} . It relates the integrated intensity, which is redistributed upon the reaction to the integrated total protein absorbance. Half of the sum of the integrated positive and negative difference bands is divided by the integrated total protein absorbance.

$$\text{COBSI index} = \frac{\int_{1610}^{1700} 0.5|\Delta\text{Abs}|d\tilde{\nu}}{\int_{1610}^{1700} \text{Abs} d\tilde{\nu}} \quad (\text{Eq. 1})$$

If two states with large differences in the spectrum are compared, the integrated total protein absorbance is the averaged value of the two states. This assures that the same COBSI index is obtained for the forward and the backward reaction.

The COBSI index is 1 if the total absorbance in the amide I region of a protein is shifted strongly in going from state A to state B so that there is no overlap between the absorbance spectra of states A and B. If 20% of the backbone C=O groups in a protein experience such a shift in absorbance, the COBSI index will be 0.2. However, in most cases there will be significant overlap of the absorption spectra of the two states, the overlap being most pronounced for, for example, subtle changes of hydrogen bonding and being less for a change in secondary structure. Therefore, in order to relate COBSI indices to changes of structure, COBSI indices for defined structural transitions were calculated from absorbance spectra in the literature. These and the COBSI indices for the ATPase reactions are collected in Table II.

COBSI indices for secondary structure transitions between 100% α -helix, β -sheet, and turn structure or transitions from an ordered to an unordered structure are in the range 0.2–0.6, indicating that 20–60% of the integrated absorbance is redistributed upon such a transition. As expected, a lower value of 0.09 is obtained when antiparallel and parallel β -sheets are compared because the backbone is in an extended conformation in both cases, and the spectral differences may therefore mainly be caused by changes of hydrogen bonding.

The COBSI indices for the ATPase partial reactions investigated here are of the order of 10^{-3} to 10^{-4} . Assuming half of the total protein being active ATPase (based on typically 4–5 nmol of active ATPase/mg of protein; Refs. 19–25), the ATPase COBSI indices have to be multiplied by a factor of 2 and are then near a value of 0.002. This is more than 2 orders of magnitude smaller than COBSI indices for a 100% secondary

TABLE II
Change of backbone structure and interaction (COBSI) index for ATPase reactions and for selected conformational changes of other proteins or peptides
The calculation of COBSI indices is described under "Discussion."

System	Reaction	Reference	COBSI index/10 ⁻³			
			H ₂ O		² H ₂ O	
			Type I samples ^a	Type II samples ^a	Type I samples ^a	Type II samples ^a
Ca ²⁺ ATPase	ATP binding	This work	1.00	0.64	1.24	1.04
	Phosphorylation	This work	0.40	0.28	0.37	0.70
	Conversion	This work		0.80		0.80
	Ca ²⁺ binding	(9)		0.85		0.90
	Thermal denaturation	(60)		18.5		44.3
Set of proteins used to calculate spectra of pure α -helical, β -sheet and turn structure	α -Helix \leftrightarrow β -sheet ^b	(61, 62)	192, 211			
	α -Helix \leftrightarrow turn ^b	(61, 62)	245, 151			
	α -Helix \leftrightarrow turn ^b	(61, 62)	245, 151			
	β -Sheet \leftrightarrow turn ^b	(61, 62)	368, 327			
Set of peptides used to calculate spectra of pure α -helical, β -sheet and unordered structure	$\beta^- \leftrightarrow \beta^+$	(62)	91			
	β -Sheet \leftrightarrow unordered	(61)	567			
Ac-(AAAK) ₄ -NH ₂ (peptide K4)	α -Helix \leftrightarrow unordered	(63)			255	
	β -Sheet \leftrightarrow unordered	(46, 47)	566		664	

^a The discrimination between type I samples and type II samples refers only to the reactions investigated in this work.

^b First value is derived from Ref. 61, the second value from Ref. 62. Values obtained from the latter reference for parallel (β^+) and antiparallel (β^-) sheet structures were averaged. The deviation from the average value was less than 10%.

structure transition indicating that the ATPase secondary structure is virtually unperturbed by Ca^{2+} binding, ATP binding, ATPase phosphorylation, and phosphoenzyme conversion. Relating the value of 0.002 for the ATPase partial reactions to the values of 0.2–0.6 of a secondary structure change involving all residues, we estimate that the net change of secondary structure as seen by infrared spectroscopy involves 0.3–1% of the ATPase residues, *i.e.* 3–10 amino acids. This estimate does not rule out the possibility that the secondary structure is entirely preserved in all reaction steps and the absorbance differences arise from subtle changes of hydrogen bonding. A similar conclusion was previously reached by us using a simpler approach, involving a smaller number of partial reactions and based upon spectra obtained in a more indirect way (8).

The COBSI indices for all partial reactions of the ATPase investigated are of the same order of magnitude, leading to the conclusion that the two steps of (i) Ca^{2+} binding and (ii) phosphoenzyme conversion concomitant with Ca^{2+} release are not associated with major secondary structure changes relative to other partial reactions. Our view is that all steps investigated are associated with secondary structure changes of comparable magnitude and that it is not possible to distinguish between minor and major secondary structure changes in the catalytic cycle of the Ca^{2+} -ATPase.

The finding of only minor secondary structure changes in the catalytic cycle of the ATPase is in agreement with fluorescence energy transfer studies which do not detect changes of distances between fluorescence labels upon Ca^{2+} or vanadate binding or enzyme phosphorylation (see Refs. 50–53, and references therein). However, a recent study reported a distance change in the catalytic cycle of the Na^+/K^+ -ATPase (54). Circular dichroism experiments indicate slightly larger secondary structure changes than our infrared results, showing an increase of the signal at 225 nm of up to 5% upon Ca^{2+} binding and of 2% upon ATPase phosphorylation ($E \rightarrow E_2\text{-P}$) (55). At present, this small discrepancy cannot be resolved.

A nearly unperturbed secondary structure as observed here seems to be in conflict with recent small angle x-ray diffraction data showing a redistribution of 8% of protein mass from the cytoplasmic side of the membrane into the membrane (56). However, both methods monitor completely different proper-

ties. Small angle x-ray diffraction monitors the overall shape of the protein whereas infrared spectroscopy is sensitive to local changes in the interaction of single amide groups with their environment. If the data of the two methods are combined, a reasonable scenario is that movement of large parts of the protein is promoted by a change in backbone conformation which involves only a few amide groups and which largely preserves the existing secondary structure. Other spectroscopic methods like fluorescence (reviewed in Refs. 53, 57, and 58) and electron paramagnetic resonance (59) also reveal the conformational changes associated with the ATPase reaction cycle. The structural extent of the changes is, however, hard to quantify with these methods.

Interestingly, thermal denaturation of the ATPase (60) leads to COBSI indices which are a factor of 20–40 larger than those of the partial reactions but still about 1 order of magnitude smaller than expected for a secondary structure change of all residues. This indicates that the structure is not totally disrupted upon thermal denaturation. This is in line with the second derivative spectrum of the denatured state, which is inconsistent with an overall random coil structure. In addition, the absorbance spectrum shows that intermolecular β -sheets often observed upon protein denaturation (43) are not the dominant structure of the denatured ATPase.

CONCLUSIONS

The time-resolved infrared spectra described here present a new access to the analysis of the number of intermediates and the dynamics of their interconversion in the Ca^{2+} -ATPase reaction cycle. The use of caged compounds provides high quality infrared difference spectra of only small absorbance changes at a time resolution generally of the order of 10–100 ms. Even absorbance changes as small as 0.0002 can be used to monitor the time course of the reaction. The results provide no evidence for long-lived intermediates in the course of $E_2\text{-P}$ formation other than Ca_2E_1ATP and $\text{Ca}_2E_1\text{-P-ATP}$. For all partial reactions investigated, the secondary structure of the ATPase seems to be nearly unperturbed.

Time-resolved infrared spectroscopy based on caged compounds can easily be applied to other systems. Therefore we

expect that this approach will successfully be used for a wide range of enzyme systems.

Acknowledgments—We thank Prof. Dr. W. Hasselbach (Max-Planck-Institut, Heidelberg) for the gift of Ca^{2+} -ATPase and Dr. J. E. T. Corrie (National Institute for Medical Research, London) for the preparation of caged AMP-PNP.

REFERENCES

- Petithory, J. R., and Jencks, W. P. (1988) *Biochemistry* **27**, 5553–5564
- Andersen, J. P. (1989) *Biochim. Biophys. Acta* **988**, 47–72
- De Meis, L., and Vianna, A. (1979) *Annu. Rev. Biochem.* **48**, 275–292
- Khananshvilii, D., and Jencks, W. P. (1988) *Biochemistry* **27**, 2943–2952
- Stahl, N., and Jencks, W. P. (1987) *Biochemistry* **26**, 7654–7667
- Myung, J., and Jencks, W. P. (1995) *Biochemistry* **34**, 3077–3083
- Jencks, W. P., Yang, T., Peisach, D., and Myung, J. (1993) *Biochemistry* **32**, 7030–7034
- Barth, A., Kreutz, W., and Mäntele, W. (1994) *Biochim. Biophys. Acta* **1194**, 75–91
- Georg, H., Barth, A., Kreutz, W., Siebert, F., and Mäntele, W. (1994) *Biochim. Biophys. Acta* **1188**, 139–150
- Buchet, R., Jona, I., and Martonosi, A. (1991) *Biochim. Biophys. Acta* **1069**, 209–217
- De Meis, L., and Hasselbach, W. (1971) *J. Biol. Chem.* **246**, 4759–4763
- Barth, A., Mäntele, W., and Kreutz, W. (1991) *Biochim. Biophys. Acta* **1057**, 115–123
- Walker, J. W., Reid, G. P., McCray, J. A., and Trentham, D. R. (1988) *J. Am. Chem. Soc.* **110**, 7170–7177
- Suzuki, H., Nakamura, S., and Kanazawa, T. (1994) *Biochemistry* **33**, 8240–8246
- Shigekawa, M., Wakabayashi, S., and Nakamura, H. (1983) *J. Biol. Chem.* **258**, 8698–8707
- Lacapere, J.-J., and Guillain, F. (1990) *J. Biol. Chem.* **265**, 8583–8589
- Shigekawa, M., and Dougherty, J. P. (1978) *J. Biol. Chem.* **253**, 1458–1464
- Yamada, S., and Ikemoto, N. (1980) *J. Biol. Chem.* **255**, 3108–3119
- Inesi, G., and Kurzmack, M. (1984) in *Topics in Molecular and Structural Biology: Biomembrane Structure and Function* (Chapman, D., ed) Vol. 4, pp. 355–410, Verlag Chemie, Weinheim, Germany
- Inesi, G., and De Meis, L. (1985) in *The Enzymes of Biological Membranes* (Martonosi, A., ed) 2nd Ed., Vol. 3, pp. 157–191, Plenum Press, New York
- Inesi, G. (1987) *J. Biol. Chem.* **262**, 16338–16342
- Nakamura, Y., and Tonomura, Y. (1982) *J. Biochem. (Tokyo)* **91**, 449–461
- Fernandez-Belda, F., Kurzmack, M., and Inesi, G. (1984) *J. Biol. Chem.* **259**, 9687–9698
- Andersen, J. P., Lassen, K., and Møller, J. V. (1985) *J. Biol. Chem.* **260**, 371–380
- Shigekawa, M., Wakabayashi, S., and Nakamura, H. (1983) *J. Biol. Chem.* **258**, 14157–14161
- Shigekawa, M., Dougherty, J. P., and Katz, A. M. (1978) *J. Biol. Chem.* **253**, 1442–1450
- Makinose, M. (1969) *Eur. J. Biochem.* **10**, 74–82
- Pickart, C. M., and Jencks, W. P. (1984) *J. Biol. Chem.* **259**, 1629–1643
- Petithory, J. R., and Jencks, W. P. (1986) *Biochemistry* **25**, 4493–4497
- Linse, S., Jonsson, B., and Chazin, W. J. (1995) *Proc. Natl. Acad. Sci. U. S. A.* **92**, 4748–4752
- Barth, A., Hauser, K., Mäntele, W., Corrie, J. E. T., and Trentham, D. R. (1995) *J. Am. Chem. Soc.* **117**, 10311–10316
- Von Gernar, F. (1994) *Investigation of the Nucleotide Binding Site of the Sarcoplasmic Reticulum Ca^{2+} -ATPase*. Diplom thesis, University of Freiburg, Germany
- Champeil, P., Rioulet, S., Orłowski, S., Guillain, F., Seebregts, C. J., and McIntosh, D. B. (1988) *J. Biol. Chem.* **263**, 12288–12294
- Shigekawa, M., and Dougherty, J. P. (1978) *J. Biol. Chem.* **253**, 1451–1457
- Wakabayashi, S., Ogurusu, T., and Shigekawa, M. (1986) *J. Biol. Chem.* **261**, 9762–9769
- Champeil, P., and Guillain, F. (1986) *Biochemistry* **25**, 7623–7633
- Brandl, C. J., Green, N. M., Korczak, B., and MacLennan, D. H. (1986) *Cell* **44**, 597–607
- Isaacs, N. S. (1987) *Physical Organic Chemistry*, pp. 255–281, Longman, Harlow UK
- Schowen, K. B., and Schowen, R. L. (1982) *Methods Enzymol.* **87**, 551–606
- Urbauer, J. L., Dorgan, L. J., and Schuster, S. M. (1984) *Arch. Biochem. Biophys.* **231**, 498–502
- Dorgan, L. J., and Schuster, S. M. (1981) *J. Biol. Chem.* **256**, 3910–3916
- Arrondo, J. L. R., Muga, A., Castresana, J., and Goni, F. M. (1993) *Prog. Biophys. Mol. Biol.* **59**, 23–56
- Jackson, M., and Mantsch, H. H. (1995) *Crit. Rev. Biochem. Mol. Biol.* **30**, 95–120
- Harris, P. I., and Chapman, D. (1994) in *Methods in Molecular Biology: Microscopy, Optical Spectroscopy, and Macroscopic Techniques* (Jones, C., Mulloy, B., and Thomas, A. H., eds) Vol. 22, pp. 183–202, Humana Press Inc., Totowa, NJ
- Sarver, R. W. J., and Krueger, W. C. (1991) *Anal. Biochem.* **194**, 89–100
- Venyaminov, S. Y., and Kalnin, N. N. (1990) *Biopolymers* **30**, 1259–1271
- Chirgadze, Y. N., Shestopalov, B. V., and Venyaminov, S. Y. (1973) *Biopolymers* **12**, 1337–1351
- Venyaminov, S. Y., and Kalnin, N. N. (1990) *Biopolymers* **30**, 1243–1257
- Chirgadze, Y. N., Fedorov, O. V., and Trushina, N. P. (1975) *Biopolymers* **14**, 679–694
- Stefanova, H. I., Mata, A. M., East, J. M., Gore, M. G., and Lee, A. G. (1993) *Biochemistry* **32**, 356–362
- Baker, K. J., East, J. M., and Lee, A. G. (1994) *Biochim. Biophys. Acta* **1192**, 53–60
- Stefanova, H. I., Mata, A. M., Gore, M. G., East, J. M., and Lee, A. G. (1993) *Biochemistry* **32**, 6095–6103
- Bigelow, D. J., and Inesi, G. (1992) *Biochim. Biophys. Acta* **1113**, 323–338
- Lin, S. H., and Faller, L. D. (1996) *Biochemistry* **35**, 8419–8428
- Girardet, J. L., and Dupont, Y. (1992) *FEBS Lett.* **296**, 103–106
- Blasie, J. K., Herbette, L. G., Pascolini, D., Skita, V., Pierce, D. H., and Scarpa, A. (1985) *Biophys. J.* **48**, 9–18
- Kanazawa, T., Suzuki, H., Daiho, T., and Yamasaki, K. (1995) *Biosci. Rep.* **15**, 317–326
- Ferreira, S. T., and Coelho-Sampaio, T. (1996) *Biosci. Rep.* **16**, 87–106
- Mahaney, J. E., Froehlich, J. P., and Thomas, D. D. (1995) *Biochemistry* **34**, 4864–4879
- Jaworsky, M., Brauner, J. W., and Mendelsohn, R. (1986) *Spectrochim. Acta* **42A**, 191–198
- Kalnin, N. N., Baikov, I. A., and Venyaminov, S. Y. (1990) *Biopolymers* **30**, 1273–1280
- Pribic, R., Van Stokkum, I. H. M., Chapman, D., Harris, P. I., and Bloemendal, M. (1993) *Anal. Biochem.* **214**, 366–378
- Martinez, G., and Hillhauser, G. (1995) *J. Struct. Biol.* **114**, 23–27